SMSE Waveform Design Using Soft Decision Selection and Dynamic Assignment of Subcarrier Modulation Order and Power

Eric Like[1], Michael Temple[1], and Zhiqiang Wu[2]
Air Force Institute of Technology[1], Wright State University[2]
Email: michael.temple@afit.edu

***Abstract*—Spectrally Modulated, Spectrally Encoded (SMSE) waveforms have demonstrated considerable practical utility and remain a viable alternative for Cognitive Radio (CR) -based Software Defined Radio (SDR) applications. As demonstrated in this paper, this utility is greatly enhanced when soft decision selection and dynamic assignment of SMSE design parameters is incorporated. This paper provides the analytical development for optimizing SMSE performance in a coexistent environment containing Primary User (PU) signals. Optimization is performed by exploiting statistical knowledge of PU spectral and temporal behavior, and independently selecting SMSE *intra-symbol* subcarrier power and modulation order using soft decision criteria. It is shown that SMSE system throughput can be maximized while adhering to SMSE and PU bit error rate (BER) constraints while limiting mutual coexistent interference to manageable levels. For proof-of-concept demonstration, simulation results are presented for SMSE coexistent scenarios containing DSSS and OFDM-based 802.11a PU signals. A sensitivity analysis is also provided to show performance changes resulting from variation in SMSE waveform update latency and update interval. Relative to a spectrally-only adapted waveform, the spectrally-temporally adapted SMSE waveform provides significant performance improvement. Maximum improvement is achieved using statistic-based prediction of PU channel temporal conditions and the appropriate SMSE waveform design update interval.**

***Index Terms*—Coexistence, OFDM, SMSE, Opportunistic Spectrum Access, Dynamic Spectrum Access, Waveform Agility, Adaptive Modulation.**

I. INTRODUCTION

Within the field of communications, there exists an ever growing demand for greater system performance amidst an apparent shortage of available spectrum. Stated more accurately, the spectrum remains largely under-utilized with some suggesting that 70% to 95% is inefficiently utilized at any point in time [1]–[3]. As such, the research emphasis remains focused on using existing resources more efficiently rather than demanding more. Both Cognitive Radio (CR) and Software Defined Radio (SDR) technologies are widely recognized as having considerable potential for alleviating apparent spectrum shortages [4], [5], with some of the more efficient approaches coupling intelligent CR algorithmic control with a flexible SDR system architecture. These future CR-based SDR communication systems are even more promising when they exploit the design flexibility and computational efficiency of Orthogonal Frequency Division Multiplexing (OFDM) [6].

In wireless communications, signals are designed to "coexist" within various physical domains (time, frequency, space, polarization and code). The design challenge is to provide "peaceful" coexistence such that mutual interference is manageable by all users. In the context of CR-based SDR waveforms, signal coexistence is obtained through waveform tailoring, or dynamic design, and provides interference performance that can be characterized through *overlay*, *underlay*, or hybrid *overlay-underlay* mechanisms. The specific waveform characterization is determined by comparing CR and Primary User (PU) signal characteristics in the jointly occupied physical domain(s). Basic CR-based SDR waveform characterization can be summarized as follows: 1) An *overlay* waveform design *avoids* interference by occupying areas within physical domain(s) where PU signals do not exist; 2) An underlay waveform design occupies the same areas within the physical domain(s) while inducing "manageable" interference to the PUs; and 3) A hybrid *overlay-underlay* waveform achieves both interference avoidance and management [7]–[9].

This work addresses *coexistent* CR-based SDR waveform design in a PU signal environment using OFDM-based Spectrally Modulated, Spectrally Encoded (SMSE) waveforms [10], [11]. Relative to previous related work that considered similar design constraints [12], [13], this paper provides: 1) a detailed analytical development for soft decision selection and dynamic assignment of SMSE subcarrier modulation order and power, 2) a sensitivity analysis for SMSE parameter update latency and update interval, and 3) proof-of-concept demonstrations for two different PU environments. Results here demonstrate potential performance improvement that can be realized through adaptive design of temporally and spectrally agile SMSE waveforms. By exploiting statistical knowledge of PU spectral and temporal behavior, SMSE system throughput is maximized while adhering to both SMSE and PU bit error rate (BER) constraints. Section II introduces the framework used to design temporally and

Manuscript received April 14, 2009; revised August 16, 2009; accepted August 30, 2009.

doi:10.4304/jcm.4.10.766-780

spectrally agile signals. The adaptive waveform design process is developed in Section III, focusing on the temporal and spectral statistics of PU signals as well as manageable interference levels for both the SMSE and PU systems. Simulation results are provided in Section V and Section VI for coexistent scenarios containing temporally unstructured Direct Sequence Spread Spectrum (DSSS) PU signals and temporally structured 802.11a signals, respectively. In Section VIII, the performance sensitivity to SMSE waveform update latency and update interval is investigated and the resultant trade-space explored. Section IX provides a summary and conclusions.

II. Spectral Waveform Design

A. OFDM-Based Design Methods

Orthogonal Frequency Division Multiplexing is a key technology for implementing spectrally efficient SDR [4] and posses inherent frequency agility through the use of a spectral domain design process [6]. OFDM effectively divides the total available bandwidth (B_T) among N_f narrower subcarriers, with each subcarrier modulated by independent data streams. Due to the lower bandwidth allocated to each subcarrier, the time duration of each OFDM symbol (T_S) is increased when compared to single carrier techniques using the same B_T. However, due to the parallel nature of OFDM, approximately the same data rate (R_D) can be achieved. One benefit of this process is that spectral regions within B_T that have either poor channel quality or contain high interference levels can be avoided in favor of spectral regions having better channel responses and reduced interference. Additionally, through proper selection of OFDM parameters, frequency selective channels that would have distorted the signal from a single high rate data stream can appear as frequency flat channels to each of an OFDM system's narrow subcarriers. These aspects of OFDM provide the foundation of OFDM's ability to spectrally design its signal to achieve coexistence with other users while simultaneously maximizing its own throughput and performance.

Adaptive methods have been proposed for OFDM-based communication systems in order to spectrally adapt to changing channel conditions while increasing performance in the presence of other users. The complexity of these designs ranges from simple spectral notching (avoid spectral regions with high interference or poor channel gain) to theoretically optimal methods, such as water-filling, that strive to achieve Shannon capacity [14], [15]. These methods generally suffer from either limited performance capability or unrealistic design constraints. Some of the more practical adaptive techniques employ traditional modulation schemes with subcarrier adaptability provided on either an *inter-symbol* (symbol-to-symbol) or *intra-symbol* (within a symbol) basis. The inter-symbol class of signals, e.g., OFDM-based 802.11 [16], typically use fixed assignment of modulation type, order, etc., for all subcarriers within a given symbol. Signals using intra-symbol adaptability vary subcarrier properties within each symbol. This has been used in both wired [17]–[19] and wireless applications [20]–[23] that have predominantly used *spectral-only* design to maximize OFDM system throughput without due regard to coexistent system impact. As a result, their utility diminishes in the presence of PU systems which require a given performance level. Thus, greater design flexibility through independent selection of OFDM subcarrier features is required.

B. SMSE Analytic Framework

Fundamental research has been completed that provides a unified framework to aid in the spectral design of OFDM signals. The so-called Spectrally Modulated Spectrally Encoded (SMSE) framework in [10], [11], reduces the generally complex spectral design of OFDM signals down to the selection of six key parameters. Each SMSE parameter is introduced to incorporate various waveform design characteristics commonly employed in communications. While the design of OFDM spectral components can be accomplished by various means, the SMSE framework provides a concise methodology for describing OFDM signals through various SMSE parameters.

The general SMSE framework specifies the transmitted waveform design for the k^{th} SMSE symbol using a specific collection of waveform design parameters, including: *coding*, $\mathbf{c} = [c_1, c_2, \ldots, c_{N_f}], c_i \in \mathbb{C}$, *data modulation*, $\mathbf{d} = [d_1, d_2, \ldots, d_{N_f}], d_i \in \mathbb{C}$, *windowing*, $\mathbf{w} = [w_1, w_2, \ldots, w_{N_f}], w_i \in \mathbb{C}$, and a phase-only *orthogonality* term, $\mathbf{o} = [o_1, o_2, \ldots, o_{N_f}]$, $o_i \in \mathbb{C}$, $|o_i| = 1 \ \forall \ i$ [10], [11]. Collectively, these terms functionally incorporate various waveform design features that are commonly employed in communications. The intra-symbol frequency components used to generate each SMSE symbol are controlled by the *assignment*, $\mathbf{a} = [a_1, a_2, \ldots, a_{N_f}]$, $a_i \in \{0, 1\}$, and *use*, $\mathbf{u} = [u_1, u_2, \ldots, u_{N_f}]$, $u_i \in \{0, 1\}$ parameters, where zeros indicate there is no transmission at that particular frequency. The *assignment* parameter specifies available frequency bands, while the *use* parameter dictates which ones are actually used. Thus, $\mathbf{u}$ is a subset of $\mathbf{a}$, $\mathbf{u} \subseteq \mathbf{a}$, such that only assigned carriers can be used.

The spectral representation of the k^{th} SMSE symbol is given by [10], [11]

$$\mathbf{s}_k = \mathbf{a}_k \odot \mathbf{u}_k \odot \mathbf{c} \odot \mathbf{d}_k \odot \mathbf{w} \odot \mathbf{o}_k \ , \tag{1}$$

where $\odot$ denotes a Hadamard product. The m^{th} subcarrier component of $\mathbf{s}_k$ is given as

$$\mathbf{s}_k[m] = a_{m,k} u_{m,k} c_m d_{m,k} w_m \mathrm{e}^{j\Theta_{m,k}}, \tag{2}$$

$$\Theta_{m,k} = \theta_{c_m} + \theta_{d_{m,k}} + \theta_{w_m} + \theta_{o_{m,k}} \ ,$$

where $m = 0, 1, ..., N_f - 1$ is the subcarrier index number, there are N_f total subcarriers, and $a_{m,k}$, $u_{m,k}$, c_m, θ_{c_m}, $d_{m,k}$, $\theta_{d_{m,k}}$, w_m, θ_{w_m} and $\theta_{o_{m,k}}$ are corresponding magnitudes and phases of the design parameters.

C. Soft Decision SMSE (SD-SMSE)

The general SMSE framework has been extended in recent work to allow for soft decision SMSE (SD-SMSE)

implementation [24]–[26]. In SD-SMSE, the original hard-decision restriction on SMSE *assignment* (**a**) and *use* (**u**) parameters (on or off) is relaxed and a range of continuous non-negative real values applied. For the form of SD-SMSE considered here, elements of the *assignment* sequence $\{\mathbf{a}\}$ and *use* sequence $\{\mathbf{u}\}$ include values of $a_i \in [0,1]$ and $u_i \in [0,1]$. In the context of this more general SD-SMSE framework, the desired soft decision effects include: 1) the *assignment* parameter indicating the total amount of power that the SD-SMSE system is allowed to allocate in specific spectral regions, with $a_i = 1$ indicating maximum possible (normalized) transmission power; and 2) the *use* parameter indicating the fraction of total available transmission power that is actually used across all possible spectral regions. Accounting for these two effects, the total (normalized) power transmitted on the i^{th} subcarrier is $P_i = (a_i u_i)^2 \times |c_i d_i w_i|^2$.

Development of the SD-SMSE framework naturally follows that of the original SMSE framework, with the spectral representation remaining unchanged from that given in (1) and (2). The framework in (2) is well-suited for optimization given that independent selection of intra-symbol subcarrier power and modulation type/order is enabled through the $u_{m,k}$ and $d_{m,k}$ design parameters, respectively. Since the SMSE parameters for each subcarrier are independent from those applied to all others, each subcarrier can have independent power level and modulation assigned. Furthermore, the subcarrier power and modulation can be dynamically modified on a symbol-by-symbol basis in response to changing channel and/or interference conditions. The end result is the ability to explicitly design a signal that is both time agile across symbols and frequency agile across subcarriers.

III. SD-SMSE Waveform Design

A. Spectral Design

SMSE system performance is maximized subject to specific design constraints. For this work, the imposed design constraints include: 1) Fixed total average SMSE power (summed across all subcarriers), 2) Fixed maximum SMSE BER (for all subcarriers), and 3) Fixed maximum BER for each PU signal. For demonstration, the design is further constrained to operate with a predetermined set of N_f contiguous *assigned* frequencies, with *coding* (**c**), *windowing* (**w**), and *orthogonality* (**o**) terms in (1) set to unity. The subcarrier modulations are selected independently and set to 4-QAM, 16-QAM, 64-QAM, or 256-QAM. Thus, the final design process involves optimal selection of *data modulation* (**d**) and frequency *use* (**u**) parameters. Specifically, within the overall goal of maximizing average throughput (bits/sec), the SMSE system first selects which subcarriers are used. For each selected subcarrier, the SMSE system then selects 1) the modulation order ($M \in \{4, 16, 64, 256\}$) and 2) allocated power. The spectral design constraints for the k^{th} SMSE symbol are expressed as:

$$Max \left\{ \mathbf{E} \left[\sum_{m=0}^{N_f-1} \{\mathbf{s}_k[m] \ \ \text{Bits / Symbol}\} \right] \right\} , \quad (3)$$

such that

$$\mathbf{E} \left[\sum_{m=0}^{N_f-1} \{\mathbf{s}_k[m] \ \ \text{Power}\} \right] \leq \Lambda_P , \quad (4)$$

$$\mathbf{E} \left[\sum_{m=0}^{N_f-1} \{\mathbf{s}_k[m] \ \ \text{Interference}\} \right] \leq \Lambda_{I_v} , \quad (5)$$

where Λ_P is the total average SMSE symbol power, $v \in \{1, \ldots, N_{PU}\}$, N_{PU} is the total number of PUs, Λ_{I_v} is the maximum *effective* interference power (after passing through the PU receive filter) that the v^{th} PU can tolerate from the SMSE and still maintain its BER limit, and $\mathbf{E}[\bullet]$ denotes the expectation operator. If the spectral constraints in (3) through (5) are viewed *deterministically* with respect to the *current* channel response, they can be expressed as:

$$\underset{M_m = \left\{ \substack{1,4,16,\\ 64,256} \right\}}{Max} \left\{ \mathbf{E} \left[\sum_{m=0}^{N_f-1} \log_2(M_m) \right] \right\} , \quad (6)$$

such that

$$\mathbf{E} \left[\sum_{m=0}^{N_f-1} P_m(M_m, H_m) \right] \leq \Lambda_P , \quad (7)$$

$$\mathbf{E} \left[\sum_{m=0}^{N_f-1} I_m^v(M_m, H_m) \right] \leq \Lambda_{I_v} , \quad (8)$$

where M_m is the m^{th} subcarrier modulation order, $P_m(M_m, H_m)$ is the power transmitted on the m^{th} subcarrier using modulation order M_m, H_m is the observed channel gain on the m^{th} subcarrier, and $I_m^v(M_m, H_m)$ is the resultant *effective* interference power observed by the v^{th} PU due to the m^{th} SMSE subcarrier (after passing through the PU receive filter). Note that $M_m = 1$ is introduced in (6) to account for *unused* subcarriers, as identified by zero entries in SMSE variable **u** in (1), with $P_m(M_m, H_m) \equiv 0$ when $M_m = 1$.

The interference power limit, Λ_{I_v} in (8), can be computed from the BER equation for the v^{th} PU system. Approximating the interference from the SMSE signal as Gaussian, and assuming the PU uses a rectangular QAM or coherent BPSK signal, the uncoded PU BER is [27]:

$$P_{b_v} \approx C_{PU} \times Q \left(\sqrt{\frac{3 \ \text{SINR}_{PU}}{2(\alpha M_{PU} - 1)}} \right) \quad (9)$$

$$C_{PU} \equiv \frac{4(\sqrt{\alpha M_{PU}} - 1)}{\sqrt{\alpha M_{PU}} \log_2(\alpha M_{PU})}$$

$$\text{SINR}_{PU} \equiv \frac{2 \log_2(\alpha M_{PU}) E_{b_v}}{N_0 + 2 \sum_{m=0}^{N_f-1} I_m^v(M_m, H_m)}$$

where M_{PU} is the modulation order used by the PUs, $N_0/2$ is the noise power spectral density, E_{b_v} is the energy used by the PU for each transmitted bit, and α is a constant set to $\alpha = 1$ for QAM or $\alpha = 2$ for BPSK. Rearranging the terms in (9) gives

$$\sum_{m=1}^{N_f-1} I_m^v(M_m, H_m) \leq \Lambda_{I_v} \tag{10}$$
$$\approx \frac{3\log_2(\alpha M_{PU})E_{b_v}}{2(\alpha M_{PU}-1)} \left[Q^{-1}\left(\frac{P_{b_m}}{C_{PU}}\right)\right]^{-2} - \frac{N_0}{2}$$

where $Q(\cdot)$ is given by

$$Q(x) \equiv \frac{1}{\sqrt{2\pi}} \int_x^\infty \mathrm{e}^{\frac{-y^2}{2}} \mathrm{d}y. \tag{11}$$

The resultant interference power observed by the v^{th} PU due to the m^{th} SMSE subcarrier, $I_m^v(M_m, H_m)$, can be obtained either through a priori knowledge of the PU transmission statistics, or by monitoring PU transmissions and forming estimates based on the PU channel access characteristics and PSD. Assuming the PU employs a matched filter receiver, the value for $I_m^v(M_m, H_m)$ can be obtained by correlating the PSD for the v^{th} PU, $Z_v(f)$, and the m^{th} SMSE subcarrier PSD, $X_m(f)$, as given by (31) in the Appendix:

$$I_m^v(M_m, H_m) = \frac{1}{P_{PU}^v} \int_{-\infty}^{\infty} Z_v(f)\ X_m(f)\ \mathrm{d}f$$
$$= \frac{P_m(M_m, H_m)}{T_S P_{PU}^v} \int_{-\infty}^{\infty} Z_v(f)\ \left|P(f - f_c - m\Delta f)\right|^2 \mathrm{d}f$$
$$\equiv P_m(M_m, H_m)\rho_m^v \tag{12}$$

where P_{PU}^v is the power of the v^{th} PU signal, f_c is the SMSE carrier frequency, Δf is the SMSE subcarrier spacing, and $P(f)$ is the Fourier Transform of the SMSE pulse shape.

Similarly, the resultant interference power observed by the m^{th} SMSE subcarrier due to the v^{th} PU, denoted $\widetilde{I}_m^v$, can be estimated by simply measuring the interference power received on each SMSE subcarrier, which is given by (30) in the Appendix as:

$$\widetilde{I}_m^v = \int_{-\infty}^{\infty} \frac{\left|\widetilde{P}(f - f_c - m\Delta f)\right|^2}{T_S}\ Z_v(f)\ \mathrm{d}f$$
$$\equiv P_{PU}^v \widetilde{\rho}_m^v \tag{13}$$

where $\widetilde{P}(f)$ is the Fourier Transform of the SMSE pulse shape after cyclic prefix removal.

To determine the required value of $P_m(M_m, H_m)$ in (7) that yields the desired subcarrier BER, consider the BER equation for the m^{th} SMSE subcarrier [27]:

$$P_{b_m} \approx C_m \times Q\left(\sqrt{\frac{3|H_m|^2 \mathrm{SINR}_m}{2(M_m - 1)}}\right) \tag{14}$$

$$C_m \equiv \frac{4(\sqrt{M_m} - 1)}{\sqrt{M_m}\log_2(M_m)}$$

$$\mathrm{SINR}_m \equiv \frac{2\log_2(M_m)E_{b_m}}{N_0 + 2\sum_{v=1}^{N_{PU}} P_{PU}^v \widetilde{\rho}_m^v}$$

which gives the desired value of $P_m(M_m, H_m)$ as

$$P_m(M_m, H_m) = \frac{\log_2(M_m)E_{b_m}}{T_S}$$
$$= \left(N_0 + 2\sum_{v=1}^{N_{PU}} P_{PU}^v \widetilde{\rho}_m^v\right) \frac{B(M_m)}{|H_m|^2} \tag{15}$$

$$B(M_m) \equiv \left[Q^{-1}\left(\frac{P_{b_m}}{C_m}\right)\right]^2 \left(\frac{M_m - 1}{3T_S}\right)$$

where E_{b_m} is the energy per bit allocated to the m^{th} subcarrier and T_S is the SMSE symbol period.

The result in (15) provides the power required to use a specific subcarrier with a given modulation order M_m. A more useful metric is the incremental power $\Delta P_{m,l}$ required to use the next higher modulation order on a specific subcarrier:

$$\Delta P_{m,l} \equiv \left(N_0 + 2\sum_{v=1}^{N_{PU}} P_{PU}^v \widetilde{\rho}_m^v\right) \frac{\Delta B_l}{|H_m|^2}\ , \tag{16}$$

$$\Delta B_l \equiv B(\gamma_l) - B(\gamma_{l-1})\ ,$$

where $\gamma_l \equiv \{4,\ 16,\ 64,\ 256\}$ for the index values $l = \{1,\ 2,\ 3,\ 4\}$, and $\gamma_0 \equiv 0$.

Using (16) removes the need to consider the modulation order being used on a particular subcarrier. Instead, each individual subcarrier can be regarded as four distinct channels each capable of transmitting two bits, and each with their own power requirement. Hence $\Delta P_{m,l}$ denotes the amount of power required to transmit an additional two bits. This reduces the problem of determining what modulation order to use for each subcarrier and what corresponding power level to assign to each P_m into the task of a deciding to either employ or not employ each "bit-pair channel", each with an independent power requirement of $\Delta P_{m,l}$. By viewing the channel in this way, a simpler and more equitable comparison can be made between channel configurations, and a single metric can be used to assess the amount of additional power that will be required for each potential pair of transmitted bits. It should also be noted that for all values of interest $\Delta B_{l+1} > \Delta B_l$, and hence $\Delta P_{m,l+1} > \Delta P_{m,l}$, as is required to ensure that the "bit-pair channels" for a particular subcarrier are selected in increasing order of l (i.e., 4-QAM, to 16-QAM, to 64-QAM, etc). As a result, (6) through (8) can be concisely expressed as

$$\underset{U_{m,l}=\{0,1\}}{Max} \left\{\sum_{m=0}^{N_f-1} \sum_{l=1}^{4} 2U_{m,l}\right\}\ , \tag{17}$$

such that

$$\sum_{m=0}^{N_f-1}\sum_{l=1}^{4}\Delta P_{m,l}U_{m,l}\leq\Lambda_P\ , \tag{18}$$

$$\sum_{m=0}^{N_f-1}\sum_{l=1}^{4}\Delta P_{m,l}\rho_m^v U_{m,l}\leq\Lambda_{I_v}\ , \tag{19}$$

where $U_{m,l}\in\{0,1\}$ indicates whether the "bit-pair channel" indexed by m and l is used. The optimization problem then reduces to selecting which "bit-pair channels" to use and which not to use by setting $U_{m,l}$ to the appropriate value. This maximization can be solved using Lagrange's method by maximizing

$$\begin{aligned}\underset{U_{m,l}=\{0,1\}}{Max}&\left\{\sum_{m=0}^{N_f-1}\sum_{l=1}^{4}L_{m,l}U_{m,l}\right\}\\&=\sum_{m=0}^{N_f-1}\sum_{l=1}^{4}\underset{U_{m,l}=\{0,1\}}{Max}\left\{L_{m,l}U_{m,l}\right\}\end{aligned} \tag{20}$$

$$L_{m,l}\equiv 1-\lambda_P\Delta P_{m,l}-\sum_{v=1}^{N_{PU}}\lambda_{I_v}\Delta P_{m,l}\rho_m^v$$

where $\lambda_P\geq 0$ and $\lambda_{I_v}\geq 0$ are the Lagrange multipliers that satisfy the constraints in (17) through (19). The above term is maximized by assigning

$$U_{m,l}=\begin{cases}1,\ L_{m,l}\geq 0\\0,\ L_{m,l}<0\end{cases}\ . \tag{21}$$

Therefore, the maximization problem is reduced to finding values of $\{\lambda_P,\lambda_{I_1},\ldots,\lambda_{I_{N_{PU}}}\}$ that satisfy the constraints. Although not a convex optimization problem, there are a number of methods that can be used to determine locally optimum values or to stochastically search for globally optimum values [28]–[30]. For proof of concept demonstration, the results presented in this paper use a gradient ascent of the Lagrange multipliers to find a locally optimum operating point. The result is a spectrally designed signal that is created in response to current channel and interference conditions.

B. Temporal Design

Additional benefit can be realized by adapting to the PU temporal responses as well. This can be achieved by monitoring PU transmissions and tracking the current "state" of each PU transmitter. This information can then be used to update the expected number of transmitting PUs during the next SMSE symbol interval. As a result, the expected amount of PU power that interferes with the SMSE signal, as well as the expected number of PUs that will experience SMSE interference, can be estimated. The OFDM subcarrier response can then be designed accordingly, enabling the SMSE system to vary its subcarrier selection, modulation, and power on a symbol-by-symbol basis, or as often as is needed and practical.

The PU signal "state" can be interpreted in numerous ways. In general, the "state" description includes any information that the SMSE system has and can maintain about PU transmission characteristics. In the simplest model, the PU "state" is modeled simply as whether or not the PU was transmitting at the end of the most recent SMSE symbol (PU is on or off). The result is a *reactive* spectrally-temporally designed SMSE waveform. In contrast to spectrally-only designed waveforms, *reactive* spectrally-temporally designed waveforms avoid spectral regions *when* and *where* PU signals are actually present. This model is suitable when the PU system operates: 1) without a fixed timing structure, or 2) if the time-varying structure is unknown.

The PU state model complexity can be described to account for both transmission condition (on or off) as well as duration (how long the PU remains in a given state). This additional knowledge enables the SMSE to statistically *predict* times that a PU is likely to transmit. As a result, the SMSE system is better able to adapt prior to experiencing interference from the PU. This *predictive* model is suitable when the PU system operates with known temporal structure, such as some defined range of allowable transmission durations or when temporal guard bands exist between successive transmissions. This information can be included as part of the state description and used to compute times that PUs are highly likely to transmit. The resultant waveform is able to avoid PU signals with an even greater degree of temporal and spectral agility as compared to the merely *reactive* case.

For any level of state complexity, the SMSE system builds a model estimate of PU signal statistics and tailors its temporal response accordingly. As with PU PSD estimation, PU temporal transmission statistics may be obtained either directly using a priori knowledge of PU signal structure, or indirectly by monitoring the PU transmissions. The SMSE system can maintain updated PU statistics and alter its response as PU signal statistics change.

Accounting for PU state conditions, the design constraints in (17) through (19) are modified such that 1) $U_{m,l}$ and $\Delta P_{m,l}$ become functions of the PU state, and 2) the potential interference power caused by the SMSE to the PU in (19) is averaged over the number of PU symbols experiencing interference. The resulting constraints become

$$\underset{U_{m,l}(\vec{D})=\{0,1\}}{Max}\left\{\int_{\vec{D}}\sum_{m=0}^{N_f-1}\sum_{l=1}^{4}2U_{m,l}(\vec{D})p(\vec{D})\,\mathrm{d}\vec{D}\right\}\ , \tag{22}$$

such that

$$\int_{\vec{D}}\sum_{m=0}^{N_f-1}\sum_{l=1}^{4}\Delta P_{m,l}(\vec{D})U_{m,l}(\vec{D})p(\vec{D})\,\mathrm{d}\vec{D}\leq\Lambda_P\ , \tag{23}$$

$$\int_{\vec{D}}\sum_{m=0}^{N_f-1}\sum_{l=1}^{4}\Delta P_{m,l}(\vec{D})\rho_m^v E_{\vec{D}}U_{m,l}(\vec{D})p(\vec{D})\,\mathrm{d}\vec{D}\leq\Lambda_{I_v}\ , \tag{24}$$

$$E_{\vec{D}} \equiv \frac{\mathbf{E}[n_v|\vec{D}]}{\mathbf{E}[n_v]} \quad , \quad p(\vec{D}) \equiv \prod_{v=1}^{N_{PU}} p(D_v) \ ,$$

where n_v is a random variable representing the number of symbols the SMSE system observes from the v^{th} PU during the next SMSE symbol interval, $\vec{D} \equiv [D_1, D_2, \ldots, D_{N_{PU}}]$ denotes the state of each PU transmitter, $p(D_v)$ is the probability density that the v^{th} PU is in the state D_v, and the integrals in (22) through (24) are taken over the range of possible PU states. The incremental power $\Delta P_{m,l}$ is now a function of PU state and is given by:

$$\Delta P_{m,l}(\vec{D}) \equiv \left(N_0 + 2 \sum_{v=1}^{N_{PU}} P_{PU}^v \widetilde{\rho}_m^v E_{\vec{D}} \right) \frac{\Delta B_l}{|H_m|^2} \ . \quad (25)$$

In the event there are only a discrete number of PU states, the probability densities become impulses and the integrals reduce to summations. By again employing Lagrange's method, this maximization can be solved by maximizing

$$\begin{aligned} &\underset{U_{m,l}(\vec{D})=\{0,1\}}{Max} \left\{ \int_{\vec{D}} \sum_{m=0}^{N_f-1} \sum_{l=1}^{4} L_{m,l}(\vec{D}) U_{m,l}(\vec{D}) p(\vec{D}) \, \mathrm{d}\vec{D} \right\} \\ &= \int_{\vec{D}} \sum_{m=0}^{N_f-1} \sum_{l=1}^{4} \underset{U_{m,l}(\vec{D})=\{0,1\}}{Max} \left\{ L_{m,l}(\vec{D}) U_{m,l}(\vec{D}) \right\} p(\vec{D}) \, \mathrm{d}\vec{D} \end{aligned} \quad (26)$$

$$L_{m,l}(\vec{D}) \equiv 1 - \lambda_P \Delta P_{m,l}(\vec{D}) - \sum_{v=1}^{N_{PU}} \lambda_{I_v} \Delta P_{m,l}(\vec{D}) \rho_m^v E_{\vec{D}}$$

where $\lambda_P \geq 0$ and $\lambda_{I_v} \geq 0$ are again the Lagrange multipliers that satisfy the constraints in (22) through (24). The expression above is maximized by assigning

$$U_{m,l}(\vec{D}) = \begin{cases} 1, & L_{m,l}(\vec{D}) \geq 0 \\ 0, & L_{m,l}(\vec{D}) < 0 \end{cases} \ . \quad (27)$$

The result is a *spectrally-temporally* designed signal created in response to the current *and* predicted channel and interference conditions. The "bit-pair channel" selection function, $U_{m,l}(\vec{D})$, is now a function of the PU state. Even though this represents a potentially uncountably infinite number of values corresponding to the possibly continuous range of PU states, the only terms that are required to be stored are the $N_{PU} + 1$ values of $\{\lambda_P, \lambda_{I_1}, \ldots, \lambda_{I_{N_{PU}}}\}$. When the SMSE computes any particular value for the PU states ($\vec{D}$), it can calculate the appropriate value of $U_{m,l}(\vec{D})$ for each m and l based on the values of λ_P and each λ_{I_v}.

IV. Estimation of Coexistent Interference

To demonstrate the ability of the SMSE to estimate the resultant coexistent interference – the interference caused by the SMSE to the PUs in (12) as well as that caused by PUs to the SMSE in (13) – the predicted coexistent interference levels are compared here to the observed values obtained through simulation.

The demonstration scenario includes a single Direct Sequence Spread Spectrum (DSSS) PU signal employing Binary Phase Shift Keying (BPSK) modulation for both data and spreading. The transmitted PU power level is fixed at 1 Watt using a symbol rate of 250K Sym/Sec, and is transmitted at a center frequency of 5.0 GHz through an Additive White Gaussian Noise (AWGN) channel. A 31-length gold code sequence is used for the spreading code with exactly one code period per BPSK data symbol.

The SMSE signal is spectrally centered at 5.0 GHz, and contains $N_f = 128$ subcarriers with each spanning 344.5 KHz and modulated using a 1 Watt QPSK signal. The SMSE signal uses a 32 length cyclic prefix and propagates through a multipath Rayleigh faded channel with a time duration equal to one-half of the SMSE cyclic prefix length.

The predicted interference observed by the PU due to the presence of the m^{th} SMSE subcarrier is shown in Fig. 1a along with the observed values obtained through simulation. Figure 1b shows the corresponding predicted and simulated interference observed by the m^{th} SMSE subcarrier due to the presence of the PU signal. In both cases, the observed simulated interference levels closely match the predicted values.

V. Coexistent Performance: Temporally *Unstructured* DSSS PU Signals

SMSE system performance is simulated in a coexistent environment containing four Direct Sequence Spread Spectrum (DSSS) PU signals. This scenario is chosen for consistency with earlier work presented in [12]. The DSSS PU signals use Binary Phase Shift Keying (BPSK) modulation for both data and spreading. The transmitted PU power level is fixed at 20 Watts per PU using a symbol rate of 300K Sym/Sec. A 32-length Hadamard sequence is used for the spreading code with exactly one code period per BPSK data symbol. The four PU signals are spectrally non-overlapped at center frequencies of 2.0120 GHz, 2.0383 GHz, 2.0680 GHz, and 2.0931 GHz. Each PU signal is generated using independent data modulation, carrier phase and symbol timing. The PU burst transmissions are modeled as exponential random variables with a mean duration of 20.0 *m*Sec for both burst length and inter-burst spacing. An AWGN channel model is used with the noise power set to achieve an in-band $SNR = 6.2$ dB.

The SMSE signal uses a maximum of $N_f = 8192$ possible subcarriers that are confined to a frequency band of 2.0000 GHz to 2.1050 GHz (105 MHz maximum bandwidth). Each subcarrier experiences independent Rayleigh flat fading through the AWGN channel. The SMSE system has a perfect channel response estimate at both the transmitter and receiver locations and updates its PU transmission state estimate prior to each SMSE symbol transmission. Furthermore, all transmitters and receivers in the scenario (PU and SMSE) are assumed

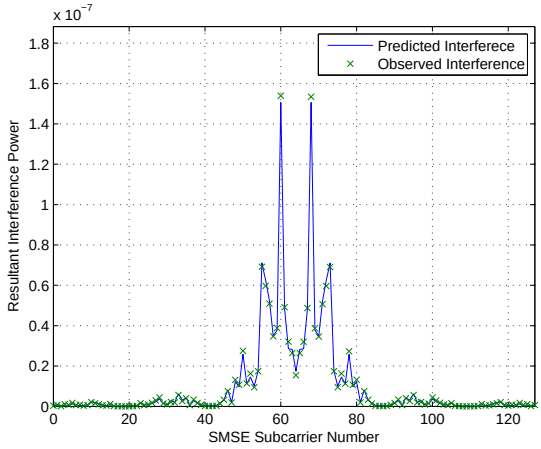

(a) Interference to the PU from the m^{th} SMSE subcarrier

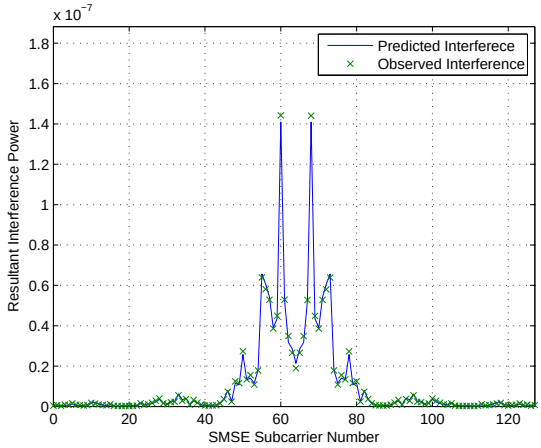

(b) Interference to the m^{th} SMSE subcarrier from the PU

Fig. 1. Predicted interference and observed interference obtained through simulation: (a) observed by the PU due to the presence of the m^{th} SMSE subcarrier and (b) observed by the m^{th} SMSE subcarrier due to the presence of the PU.

to observe the same set of signals, but with independent noise realizations. Given that the transmitted burst lengths and intervals between bursts are modeled as a "memory-less" exponential random variables, the simple "on-off" PU state model is appropriate for designing a *reactive spectrally-temporally* designed waveform. Furthermore, the SMSE is assumed to have a priori knowledge of the parameters governing the burst length and inter-burst spacing when computing PU temporal statistics, as discussed in Section III-B.

A. Time-Frequency Power Spectral Density (PSD)

The time-frequency PSD responses of the PU signals and resultant SMSE signal are shown in Fig. 2 for a representative scenario. In response to the PU signals shown in Fig. 2a, the SMSE system can design a waveform either by using only spectral adaptation constraints or by using both spectral and temporal adaptation constraints.

Considering only spectral adaptation constraints, the signal satisfying (17) through (19) avoids spectral areas

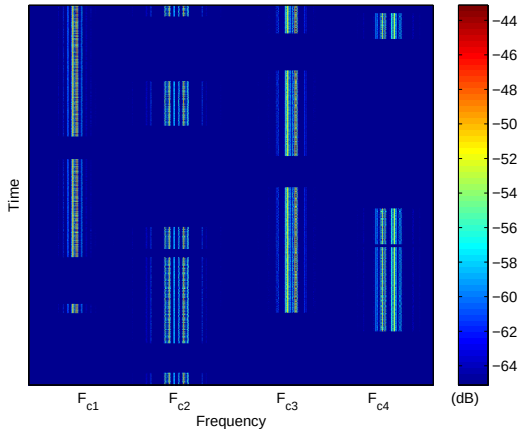

(a) DSSS PU Signal Response

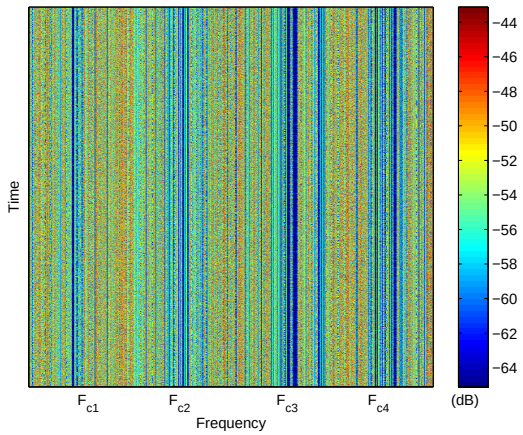

(b) SMSE Signal Response *Spectrally-Only Adapted* to PU Signal

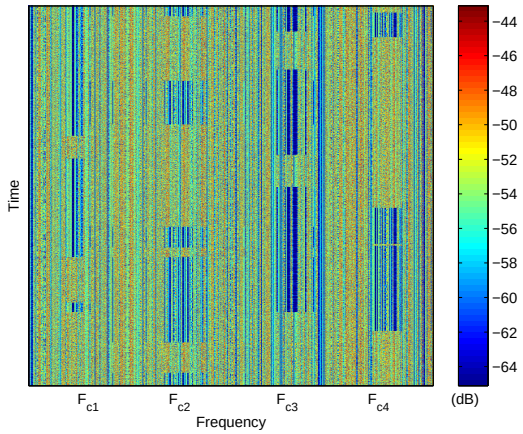

(c) SMSE Signal Response *Spectrally-Temporally Adapted* to PU Signal

Fig. 2. Coexistent *Adapted* SMSE and DSSS PU Signals. Time-Frequency PSDs: (a) Four *DSSS* PU Signals, (b) SMSE Signal Response *Spectrally-Only Adapted* to PU Signal and (c) SMSE Signal Response *Spectrally-Temporally Adapted* to PU Signal.

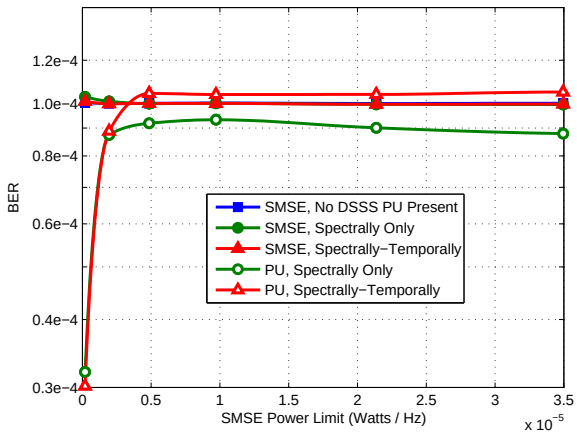

Fig. 3. Coexistent BER versus total normalized SMSE power for *Spectrally-Only* and *Spectrally-Temporally* adapted SMSE signals. Corresponding DSSS PU BER is also shown. A maximum BER constraint of $P_B = 10^{-4}$ was used for all systems.

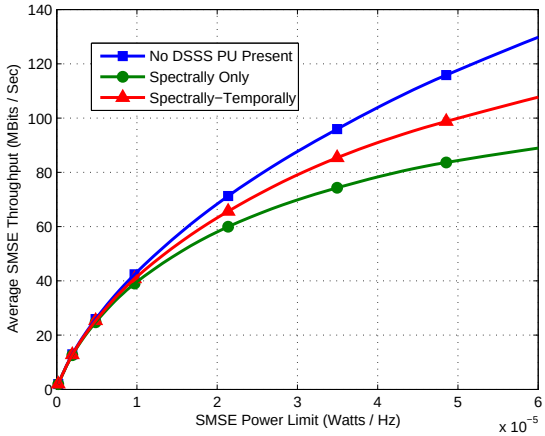

Fig. 4. Average SMSE throughput (bits/sec) versus normalized maximum SMSE power for *Spectrally-Only* and *Spectrally-Temporally* adapted SMSE signals. Results based on a maximum BER constraint of $P_B = 10^{-4}$ for all systems. Performance without the DSSS PU signals present is shown for comparison.

containing significant PU power as well as low channel gain while maximizing its throughput. The resultant *spectrally-only adapted* SMSE response in Fig. 2b clearly shows that spectral areas occupied by DSSS PU signals are avoided.

Considering both spectral and temporal adaptation constraints, the signal satisfying (22) through (24) avoids both spectral and temporal areas containing significant PU power as well as low channel gain while maximizing its throughput. This is illustrated in the time-frequency PSD response shown in Fig. 2c, where the adapted SMSE signal spectrally and temporally avoids the four DSSS PU signals using the simple "on-off" state model. The resultant *spectrally-temporally adapted* SMSE signal effectively power fills "voids" around the DSSS PU signals in both time and frequency. The SMSE response clearly avoids spectral areas where the DSSS signals are actually present.

B. PU and SMSE Bit Error Rate (BER)

Simulated PU and SMSE BER performance is shown in Fig. 3 for the spectrally-only designed SMSE waveform, and the *reactive* spectrally-temporally designed SMSE waveform. For comparison, SMSE performance is also presented without the DSSS PU signals present. Considering the SMSE BER curves (filled markers), the SMSE BER is shown to meet the desired BER limit of $P_B = 10^{-4}$ for the entire range of SMSE transmit power limits simulated, with all three curves overlapping. Considering the PU BER curves (unfilled markers) as the SMSE transmit power limit increases, the PU BER increases up to within a factor of $\pm 10\%$ of the maximum BER constraint of $P_B = 10^{-4}$. Note that this minor amount of deviation should be within the error correction capability of the PU's channel coding, and thus should be well absorbed by the channel coding. For lower SMSE power levels the PU BER is substantially lower than the BER limit. This occurs because the SMSE signal is able to select subcarrier frequencies that are considerably removed from the DSSS PU spectral regions and apply maximum power levels without causing significant interference to the PU systems.

C. Average SMSE Throughput

Results in Fig. 4 show average SMSE throughput (bits/sec) versus total maximum SMSE power (normalized by maximum SMSE bandwidth of 105 MHz) for both the *spectrally-only* and *reactive spectrally-temporally* adapted SMSE waveforms. Performance without the DSSS PU signals present is also provided for comparison. For the lower maximum total power limits considered, all three systems performed nearly identically. This occurs because the SMSE system can allocate its total power to a very few high gain channels. Therefore, when the DSSS PU signals are present, the SMSE design is effectively a simple frequency division multiplexing scheme that avoids spectral regions with high interference. Since there are generally enough high gain channels outside the DSSS PU spectral regions, the SMSE system experiences minimal penalty for avoiding the DSSS PU sub-bands. However, as total available power increases the SMSE system begins to share spectral regions with DSSS PUs and realizes a noticeable performance improvement.

VI. Coexistent Performance: Temporally *Structured* 802.11a PU Signals

Coexistent SMSE performance is analyzed in a more structured PU signal environment containing two OFDM-based 802.11a PU networks. This scenario is chosen for consistency with earlier work presented in [13]. The OFDM PU networks spann two adjacent 20 MHz channels centered at 5.00 GHz and 5.02 GHz. Consistent with specifications in [16], the 802.11a users operate as follows: 1) average transmit power fixed at $100\ mW$ per user, 2) a pre-encoded data rate of 24 Mbits/sec with a

variable length packet structure, 3) rate 1/2 forward error correction, 4) 16-QAM modulation on 48 data subcarriers, and 5) pilot tones are present. An AWGN channel model is used with the noise power set to achieve an in-band $SNR = 16.7$ dB.

The SMSE signal uses a maximum of $N_f = 128$ possible subcarriers with each spanning 344.5 KHz. The resultant overall SMSE bandwidth is 44.096 MHz centered at 5.01 GHz (spectrally centered between 802.11a bands). The SMSE signal uses a 32 length cyclic prefix and propagates through a multipath Rayleigh faded channel with a time duration equal to one-half of the SMSE cyclic prefix length. Both the PU and SMSE systems are constrained to a maximum channel BER of $P_B = 10^{-2}$. The SMSE system has a perfect channel response estimate at both the transmitter and receiver locations and updates its PU transmission state estimates every 50 SMSE symbols. Additionally, the SMSE power is further constrained to be distributed such that the resulting interference within a given 20 MHz band does not degrade PU preamble detection performance, i.e., all 802.11a users can reliably detect greater than 90% of received preambles [16].

Unlike results in Section V, results here do not rely on a priori PU information. Rather, the SMSE estimates PU transmission statistics by monitoring PU transmission activity as discussed in Section III-B. Based on these observations, the SMSE forms a histogram based estimate of the probability distribution of: 1) the PU packet transmission duration and 2) the time duration between PU packets (idle time). These probability distributions are then used to compute the conditional probabilities that the PU will remain in its current transmission state (on or off) given that it has already been in that state for some amount of time.

A. PU and SMSE Bit Error Rate

Resultant PU and SMSE channel BER versus total normalized SMSE power is shown in Fig. 5 for the *spectrally-only*, *reactive spectrally-temporally*, and *predictive spectrally-temporally* designed waveform. Considering the PU BER curves (unfilled markers) as the SMSE transmit power increases, the observed PU BER increases to the BER limit of $P_B = 10^{-2}$ for all design methods. Prior to reaching the PU BER limit, the SMSE system operates in a purely power-constrained mode, i.e., it expends its entire power budget without being impacted by the BER constraint for the PU system. As the SMSE power reaches a value of approximately $\Lambda_P = 100\ mW$, the SMSE system begins to restrict its transmission to maintain the PU BER constraint. The resultant SMSE design successfully maintains the PU BER constraint for all three design methods. Considering the SMSE BER curves (filled markers), the observed SMSE BER is consistent with the desired BER limit for both the reactive and predictive spectrally-temporally designed waveforms.

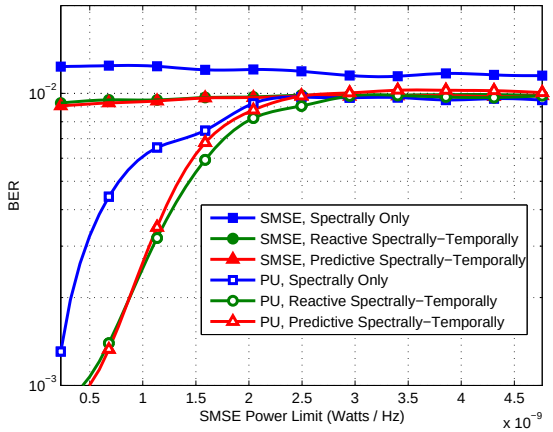

Fig. 5. Coexistent BER versus total normalized SMSE power for *Spectrally-Only*, *Reactive Spectrally-Temporally*, and *Predictive Spectrally-Temporally* adapted SMSE signals. Corresponding 802.11a PU BER is also shown. A maximum BER constraint of $P_B = 10^{-2}$ was used for all systems.

B. Average SMSE Throughput

Resultant SMSE throughput (bits/symbol) for the three design methods is shown in Fig. 6, where once again the results are plotted as a function of SMSE transmit power. As indicated, all three design methods asymptotically approach an upper limit on achievable throughput. This limitation is a result of the designs being unable to allocate all available power within the channel given that the PU BER constraint must be maintained.

The spectrally-only designed waveform achieves a significantly lower throughput than the spectrally-temporally designed waveforms. This result is partly due to the fact that spectrally-only waveform design is obtained through pure frequency division. Since this scenario has far less spectral separation between PU system than that of Section V, the SMSE waveform is less able to rely on pure frequency division to avoid PU signals. By comparison, the *reactive* spectrally-temporally designed waveform achieves an approximate 20% increase in throughput for higher power limits. For lower power limits, the *predictive* spectrally-temporally designed waveform achieves similar performance to the reactive waveform. However, as the power limit increases, the predictive waveform achieves approximately an additional 10% gain in throughput as the number of interference-free channels become scarce, and the benefit of using the PU occupied channels more efficiently becomes clear.

To illustrate SMSE subcarrier adaptability, results of SMSE subcarrier allocation are shown in Table I for the *predictive* spectrally-temporally designed waveform. Note that these results are for fixed channel noise conditions and fixed BER limit constraints of $P_B = 10^{-2}$. Given a particular channel realization, the total number of subcarriers carrying data is averaged across time, as well as the number of subcarriers employing a specific modulation order. After a minimum power limit is reached, the total

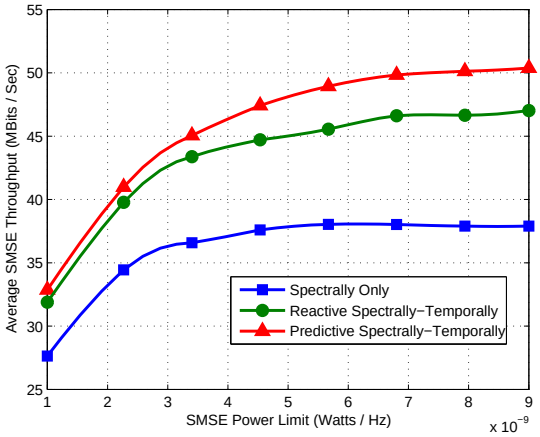

Fig. 6. Average SMSE throughput (bits/sec) versus normalized maximum SMSE power for *Spectrally-Only*, *Reactive Spectrally-Temporally*, and *Predictive Spectrally-Temporally* adapted SMSE signals. Results based on a maximum BER constraint of $P_B = 10^{-2}$ for all systems.

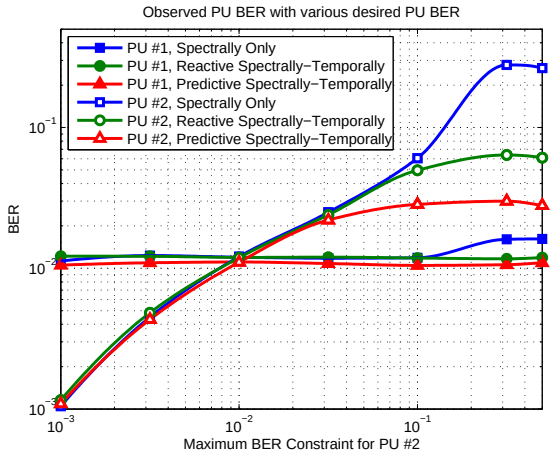

Fig. 7. Coexistent BER versus the maximum BER constraint for PU #2. Results were generated using a $P_B = 10^{-2}$ maximum BER constraint for both the SMSE and PU #1 systems.

TABLE I
SUBCARRIER UTILIZATION: AVERAGE NUMBER OF SMSE SUBCARRIERS USED AND CORRESPONDING NUMBER PER QAM MODULATION ORDER

Total SMSE Power Λ_P	Ave # Used	4 QAM	16 QAM	64 QAM	256 QAM
10 *m*W	57.66	57.66	0	0	0
50 *m*W	75.72	30.54	39.93	5.25	0
100 *m*W	75.84	28.65	22.95	24.25	0
150 *m*W	75.72	30.05	20.00	17.01	8.65
200 *m*W	75.72	32.07	18.20	10.20	15.25

number of subcarriers used remains roughly unchanged. However, as the power limit is increased, more subcarriers exchange lower-order for higher-order modulation schemes. Thus, while the total number of subcarriers used remains generally fixed to maintain the interference limit to the PU systems, the total number of resultant transmitted bits increases due to the use of higher-order modulations.

VII. DISSIMILAR PU BER CONSTRAINTS

To investigate the ability of the SMSE to design its waveform in an environment containing PUs with dissimilar BER constraints, the scenario in Section VI was modified such that the BER constraint for PU #2 (centered at 5.02 GHz) is varied while the BER constraint for PU #1 (centered at 5.00 GHz) remains fixed at $P_B = 10^{-2}$. The SMSE performance is evaluated using a maximum transmission power limit of 4.5×10^{-9} Watts/Hz.

Figure 7 shows the resultant BER observed for the two PUs as a function of the desired BER for PU #2. For the range of BER constraints considered, the resultant BER for PU #1 (filled markers) remains consistent with its design constraint of $P_B = 10^{-2}$. The resultant BER for PU #2 (unfilled markers) closely follows its desired BER constraint at lower P_B values. However, as its BER constraint increases above approximately 3×10^{-2}, the observed BER for PU #2 falls below the constraint. This is attributed to the SMSE expending all of its available transmission power before reaching the interference limit for PU #2. In all cases, the SMSE meets its own BER constraint of $P_B = 10^{-2}$.

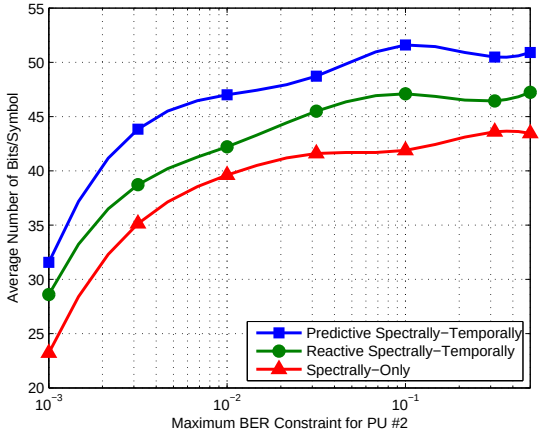

Fig. 8. Average SMSE throughput (bits/sec) versus the maximum BER constraint for PU #2. Results were generated using a $P_B = 10^{-2}$ maximum BER constraint for both the SMSE and PU #1 systems.

Resultant SMSE throughput as a function of the BER constraint for PU #2 is shown in Fig. 8. Here again, the benefit of employing a temporally agile waveform can be observed with the *predictive spectrally-temporally* designed waveform achieving the greatest throughput.

VIII. UPDATE LATENCY AND UPDATE INTERVAL

A. PU State Estimation Latency

In a practical communication design, the SMSE system will not be able to react immediately to PU transmission state changes. As a result, the PU transmission state that the SMSE uses to adaptively design its waveform will be outdated by some amount of time $\tau > 0$. If this latency is not taken into account, SMSE performance

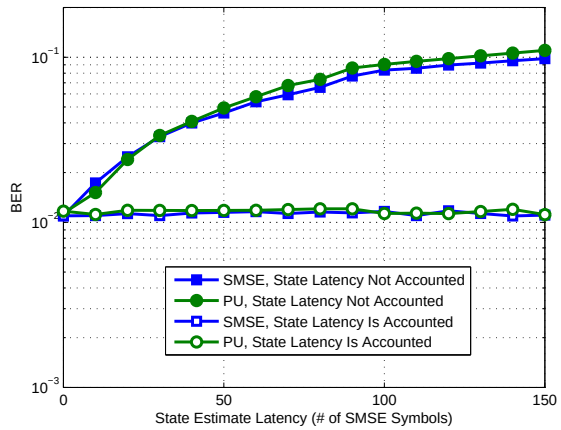

Fig. 9. Coexistent BER versus state estimation latency for *Spectrally-Temporally* adapted SMSE signal *without* latency compensation (Filled Markers) and *with* latency compensation (Unfilled Markers). Corresponding 802.11a PU BER is also shown. A maximum BER constraint of $P_B = 10^{-2}$ was used for all systems.

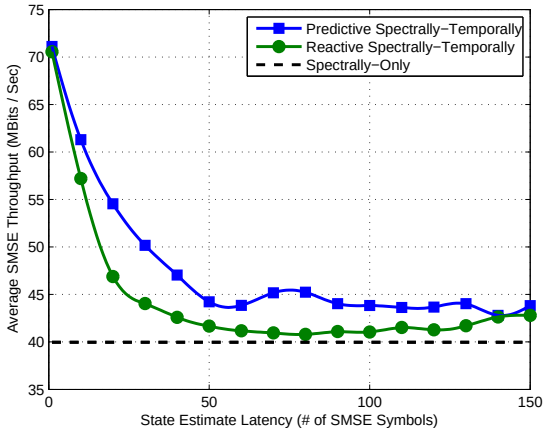

Fig. 12. Average SMSE throughput (bits/symbol) versus 802.11a PU State Estimation Latency for *Reactive Spectrally-Temporally* and *Predictive Spectrally-Temporally* adapted SMSE signals. *Spectral-Only* adapted SMSE results provided for comparison. Results based on a maximum BER constraint of $P_B = 10^{-2}$ for all systems.

will be sub-optimal for given channel conditions and mutual coexistent interference limits will not be met. This is demonstrated in Fig. 9 which shows PU and SMSE channel BER for compensated and uncompensated performance as a function of PU state estimate latency (τ), for the case of both PU BER constraints set to $P_b = 10^{-2}$.

When the SMSE waveform design process compensates for PU state estimate latency, it incorporates a decreased level of certainty about the expected amount of potential mutual interference, as well as a decrease in temporal agility incurred by its delayed response. The impact of PU state estimate latency on SMSE waveform design is illustrated in the time-frequency PSD responses in Fig. 10 and Fig. 11. In Fig. 10, the SMSE system is operated with no PU state estimate latency ($\tau = 0$) and reassigns its subcarrier power and modulation parameters prior to transmitting each symbol. The resultant response in Fig. 10b clearly exhibits three interference avoidance mechanisms, including: 1) spectral regions occupied by PU signals are only used *when* they are not present, 2) most power is allocated to spectral regions that are never occupied by PU signals (the region between the two PU channels and the right-most/left-most spectral extremes), and 3) since the OFDM-based 802.11a signals do not modulate their central subcarrier frequencies (denoted by F_{c1} and F_{c2}), the SMSE waveform allocates more power in these regions as well.

The coexistent PSD responses in Fig. 11 are for the case where the SMSE system experiences a PU state estimate latency of $\tau = 20$ SMSE symbols. Relative to $\tau = 0$ results in Fig. 10, the decreased ability of the SMSE system to quickly respond to PU state changes is clearly seen. Additionally, the increased uncertainty about the *current* PU transmission state results in less SMSE power being allocated to PU spectral regions even when the PU is not transmitting. Regarding the three interference avoidance mechanisms, the resultant SMSE response in Fig. 11a now exhibits: 1) spectral regions occupied by the PU signals only being used *when* they are not present *and* there is a low probability of the PU resuming transmission, 2) significantly more power being allocated to spectral regions that are never occupied by PU signals, and 3) more power remaining allocated in/near the PU central subcarrier frequencies (F_{c1} and F_{c2}).

SMSE system throughput is shown in Fig. 12 as a function of PU state estimate latency (τ). In this case, the SMSE system operates with a maximum average transmission power constraint of $\Lambda_P = 400\ m$W and reconfigures its subcarrier power and modulation parameters on a symbol-by-symbol basis ($K = 1$ per Section VIII-B) which enables a very high degree of temporal agility. Thus, there is limited benefit to employing a temporally predictive waveform design process. This is confirmed in Fig. 12 by the near identical performance for the two systems at $\tau = 0$. As latency increases, each system experiences an overall decrease in throughput in order to maintain desired BER performance. The benefit of employing a temporally predictive design becomes most apparent at larger values of τ. At $\tau \approx 120$ the current PU state becomes completely independent of the SMSE's outdated state estimate and all benefits of temporal agility diminish. Since the SMSE is no longer able to exploit temporal aspects of the PU signal, it effectively creates a *spectrally-only* designed waveform.

B. Update Interval Effect on Coexistent BER

A practical SMSE design needs to consider the overhead required to convey subcarrier power and modulation parameters to the intended receiver. When the SMSE system updates its waveform parameters on a symbol-by-symbol basis ($K = 1$), a considerable amount of overhead processing is required. This can be mitigated by updating SMSE parameters less frequently over blocks of

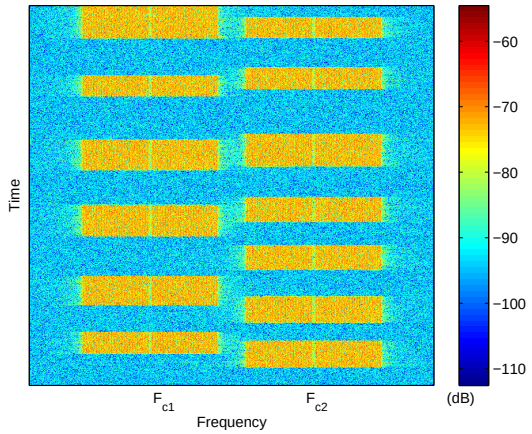

(a) OFDM-Based 802.11a PU Signal Response

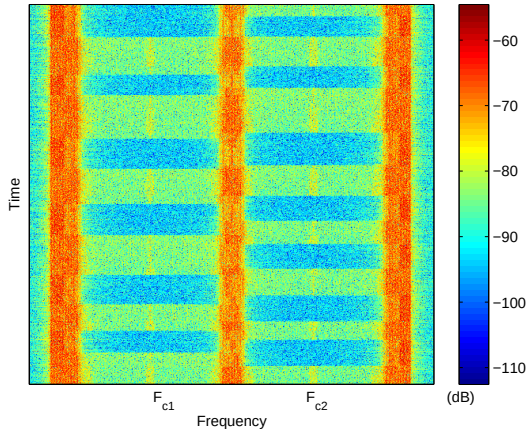

(b) Adapted SMSE Signal Response: $\tau = 0$ Symbol Latency

Fig. 10. Coexistent *Spectrally-Temporally Adapted* SMSE and OFDM-based 802.11a PU signals. PU state estimate *predictively* updated on a symbol-by-symbol basis with $\tau = 0$ symbol latency. Time-Frequency PSDs: (a) Two PU networks; (b) Adapted *SMSE* Signal.

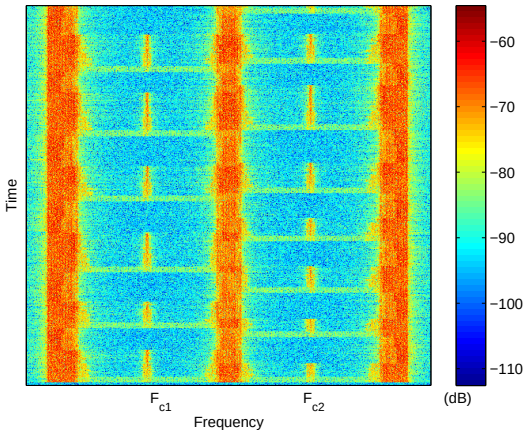

(a) Adapted SMSE Signal Response: $\tau = 20$ Symbol Latency

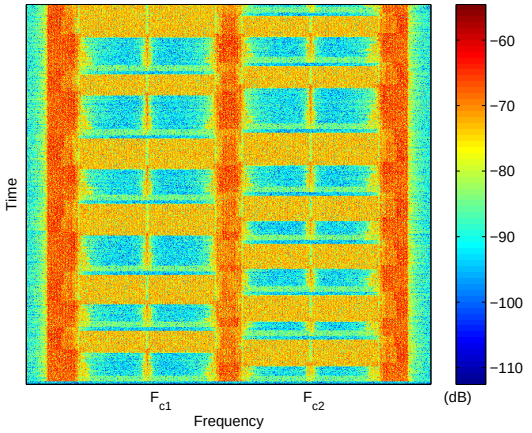

(b) Combined Coexistent Signal Response

Fig. 11. Coexistent *Spectrally-Temporally Adapted* SMSE and OFDM-based 802.11a PU signals. PU state estimate *predictively* updated on a symbol-by-symbol basis with $\tau = 20$ symbol latency. Time-Frequency PSDs: (a) Adapted *SMSE* Signal; and (b) *Combined* coexistent PU and SMSE signal response.

K symbols, for some integer $K > 1$. Relative to $K = 1$, a penalty is incurred by increasing K given that the SMSE system can only modify its response at K-symbol block boundaries. As a result, the SMSE system commits to a set of design parameters for a longer duration of time and becomes less effective at exploiting temporal gaps in PU transmissions. This increases the probability of SMSE-PU collision and mutual coexistent interference. Results in Fig. 13 demonstrate that the SMSE system is able to satisfy required BER constraints for update intervals of $K > 1$ at a maximum average transmission power of $\Lambda_P = 400$ mW. Results are shown for no PU state estimate latency ($\tau = 0$) at the start of the K-symbol interval (filled markers) as well as with state latency of $\tau = 20$ SMSE symbols (unfilled markers). For both latency cases, the BER performance of the SMSE and PU systems is consistent with the desired BER of $P_B = 10^{-2}$.

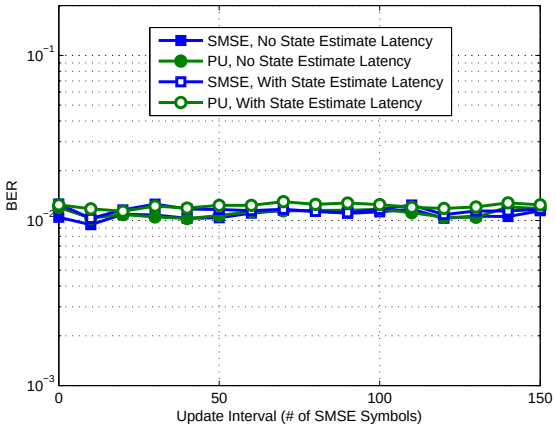

Fig. 13. Coexistent BER versus Update Interval K for *Spectrally-Temporally* adapted SMSE signal with $\tau = 0$ symbol latency (Filled Markers) and $\tau = 20$ symbol latency (Unfilled Markers). Corresponding 802.11a PU BER is also shown. A maximum BER constraint of $P_B = 10^{-2}$ was used for all systems.

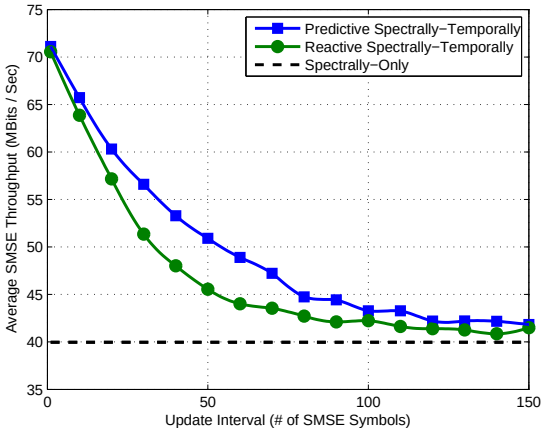

Fig. 14. Average SMSE throughput (bits/symbol) versus Update Interval K for *Predictive Spectrally-Temporally* and *Reactive Spectrally-Temporally* adapted SMSE signals with $\tau = 0$ symbol latency. *Spectral-Only* results provided for comparison. Results based on a maximum BER constraint of $P_B = 10^{-2}$ for all systems.

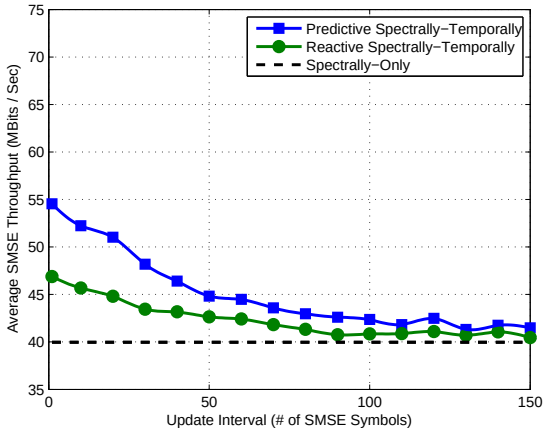

Fig. 15. Average SMSE throughput (bits/symbol) versus Update Interval K for *Predictive Spectrally-Temporally* and *Reactive Spectrally-Temporally* adapted SMSE signals with $\tau = 20$ symbol latency. *Spectral-Only* results provided for comparison. Results based on a maximum BER constraint of $P_B = 10^{-2}$ for all systems.

C. Update Interval Effect on SMSE Throughput

Results in Fig. 14 show SMSE system throughput versus SMSE update interval K with no PU state estimate latency ($\tau = 0$) at the start of the K-symbol interval. As noted earlier, for smaller values of K the SMSE system maintains a high level of temporal agility and there is only marginal benefit from employing a temporally predictive waveform design. This is confirmed in Fig. 14 by the near identical performance for the two systems at $K = 1$. As the update interval increases, each system experiences decreased throughput due to enforcement of the BER constraint. The benefit of a temporally predictive design is apparent due to the SMSE systems ability to predict future PU transmission states. However, for $K \approx 100$ and greater the SMSE system loses temporal agility and is unable to localize its designed response between consecutive PU transmissions. In this situation there is again no benefit in temporal design and throughput performance approaches that of a spectrally-only designed waveform.

Results in Fig. 15 show SMSE throughput versus update interval K using a PU state latency of $\tau = 20$ SMSE symbols and a maximum average transmission power of $\Lambda_P = 400$ mW. Relative to results in Fig. 14, there is performance degradation in the temporally-spectrally designed waveform at lower K values. The SMSE throughput performance also degrades much faster as the update interval K is increased due to the initially degraded temporal agility caused by the PU state estimate latency. If the SMSE system is unable to update its subcarrier power and modulation parameters at a shorter interval relative to results in Fig. 14, there is no benefit to designing a temporally responsive signal.

The SMSE system must therefore tradeoff conflicting design implications of the loss of throughput performance associated with: 1) the additional overhead incurred by updating the subcarrier parameters at a high rate, and 2) the degraded temporal agility due to updating the subcarrier parameters at a low rate.

IX. Summary and Conclusions

The Spectrally Modulated, Spectrally Encoded (SMSE) design process remains promising for future CR-based SDR applications. Consistent with earlier work, the practical utility of the SMSE framework is greatly enhanced through soft decision (SD) selection and dynamic assignment of SMSE design parameters. The results in this paper contribute to an expanding body of knowledge that is collectively embodied under "SD-SMSE." Of six design parameters in the SMSE framework, two were of interest in this work which focused on soft decision selection and dynamic assignment of *intra-symbol* subcarrier power and modulation order. The ultimate goal is to introduce well-designed SMSE signals into a dynamic environment containing primary users (PU) while limiting mutual coexistent interference to manageable levels.

An analytical development is provided to optimize SMSE performance in a coexistent environment containing arbitrary PU signals. The optimization exploits statistical knowledge of PU spectral and/or temporal behavior, with the SMSE waveform adapted on either a *Spectrally-Only* or *Spectrally-Temporally* basis. Proof-of-concept demonstrations are presented for two coexistent SMSE scenarios, with one including DSSS PU signals and the other including OFDM-based 802.11a PU signals. Effective SMSE waveform designs emerged in both cases, with SMSE throughput maximized and imposed BER constraints maintained on coexisting PU signals. SMSE designs are considered using both *Reactive* and *Predictive* PU state estimation and a sensitivity analysis conducted to show coexistent performance changes with variation in SMSE waveform update latency and update interval. Collectively, the *spectrally-temporally* adapted SMSE waveforms provided significant performance improvement over the *spectrally-only* adapted waveforms,

with maximum improvement achieved using *Predictive* PU state estimation.

APPENDIX
OBSERVED INTERFERENCE POWER DERIVATION

This appendix provides the derivation of formula used for estimating the effective interference power observed by a receiver after passing through a receive filter. Results here are used in support of developing (12) and (13) in Section III-A and their demonstration in Section IV. The sampled receive filter output for interfering signal $r(t)$ is given by

$$y = \frac{1}{\sqrt{T_s}} \int_{-\infty}^{\infty} h^*(t) r(t) \mathrm{d}t$$

where $1/T_s$ is the desired signal symbol rate (used to normalize the signal) and $h(t)$ is the receive filter response for the desired signal normalized to unit power $\left(\frac{1}{T_s}\int_{-\infty}^{\infty}|h(t)|^2\mathrm{d}t = 1\right)$. The received interfering signal is assumed to be of the form:

$$r(t) = \sum_{k=0}^{N-1} \sum_{m=-M}^{M} \sqrt{P_r}\alpha_k d_m g(t - mT_r - t_0 - \tau_k)$$

where P_r is interfering signal power, $1/T_r$ is the interfering signal symbol rate, $g(t)$ is its pulse shape normalized to unit power $\left(\frac{1}{T_r}\int_{-\infty}^{\infty}|g(t)|^2\mathrm{d}t = 1\right)$, t_0 is an unknown time offset which is assumed to be uniformly distributed over $[-T_r/2,\ T_r/2)$, d_m are zero-mean, unit-variance i.i.d. data modulated symbols, τ_k is the time delay of the k^{th} multipath component, α_k are complex-valued i.i.d. multipath coefficients normalized to unit power $\left(\sum_{n=0}^{N-1} E[|\alpha_n|^2] = 1\right)$, and M is an integer chosen large enough such that the interfering signal spans the support of the receive filter.

The resultant interference power is then given as

$$\begin{aligned}
E\left[|y|^2\right] &= E\left[\left|\frac{1}{\sqrt{T_s}}\int_{-\infty}^{\infty} h^*(t) r(t)\mathrm{d}t\right|^2\right] \\
&= E\left[\left|\frac{1}{\sqrt{T_s}}\int_{-\infty}^{\infty} h^*(t) \sum_{k=0}^{N-1}\sum_{m=-M}^{M}\sqrt{P_r}\alpha_k d_m \right.\right. \\
&\quad \left.\left. \times\, g(t - mT_r - t_0 - \tau_k)\mathrm{d}t\right|^2\right] \\
&= E\left[\left|\sqrt{\frac{P_r}{T_s}}\int_{-\infty}^{\infty} H^*(f) \sum_{k=0}^{N-1}\sum_{m=-M}^{M}\alpha_k d_m \right.\right. \\
&\quad \left.\left. \times\, G(f) e^{-j2\pi f(mT_r + t_0 + \tau_k)}\mathrm{d}f\right|^2\right] \\
&= E\left[\frac{P_r}{T_s}\int_{-\infty}^{\infty}\int_{-\infty}^{\infty} H^*(f)H(\xi)G(f)G^*(\xi) \right. \\
&\quad \times \sum_{\substack{\{k,l\}\\=0}}^{N-1}\sum_{\substack{\{m,n\}\\=-M}}^{M} \alpha_k\alpha_l^* d_m d_n^* \\
&\quad \left. \times\, e^{-j2\pi f(mT_r + t_0 + \tau_k)} e^{j2\pi\xi(nT_r + t_0 + \tau_l)}\mathrm{d}f\ \mathrm{d}\xi\right] \\
&= \frac{P_r}{T_s}\int_{-\infty}^{\infty}\int_{-\infty}^{\infty} H^*(f)H(\xi)G(f)G^*(\xi) \\
&\quad \times \sum_{\substack{\{k,l\}\\=0}}^{N-1} E\left[\alpha_k\alpha_l^*\right] e^{-j2\pi(f\tau_k - \xi\tau_l)} \sum_{\substack{\{m,n\}\\=-M}}^{M} E\left[d_m d_n^*\right] \\
&\quad \times \frac{1}{T_r}\int_{-\frac{T_r}{2}}^{\frac{T_r}{2}} e^{-j2\pi f(mT_r + t_0)} e^{j2\pi\xi(nT_r + t_0)}\mathrm{d}t_0\mathrm{d}f\mathrm{d}\xi \\
&= \frac{P_r}{T_s T_r}\int_{-\infty}^{\infty}\int_{-\infty}^{\infty} H^*(f)H(\xi)G(f)G^*(\xi) \\
&\quad \times \sum_{k=0}^{N-1} E\left[|\alpha_k|^2\right] e^{-j2\pi(f-\xi)\tau_k} \\
&\quad \times \sum_{m=-M}^{M} e^{-j2\pi(f-\xi)mT_r}\int_{-\frac{T_r}{2}}^{\frac{T_r}{2}} e^{-j2\pi(f-\xi)t_0}\mathrm{d}t_0\mathrm{d}f\mathrm{d}\xi \\
&= \frac{P_r}{T_s T_r}\int_{-\infty}^{\infty}\int_{-\infty}^{\infty} H^*(f)H(\xi)G(f)G^*(\xi) \\
&\quad \times \sum_{k=0}^{N-1} E\left[|\alpha_k|^2\right] e^{-j2\pi(f-\xi)\tau_k} \\
&\quad \times \frac{\sin\left[\pi(f-\xi)(2M+1)T_r\right]}{\sin\left[\pi(f-\xi)T_r\right]}\ \frac{\sin\left[\pi(f-\xi)T_r\right]}{\pi(f-\xi)}\mathrm{d}f\mathrm{d}\xi \\
&= \frac{P_r}{T_s T_r}\int_{-\infty}^{\infty}\int_{-\infty}^{\infty} H^*(f)H(\xi)G(f)G^*(\xi) \\
&\quad \times \sum_{k=0}^{N-1} E\left[|\alpha_k|^2\right] e^{-j2\pi(f-\xi)\tau_k} \\
&\quad \times \frac{\sin\left[\pi(f-\xi)(2M+1)T_r\right]}{\pi f}\mathrm{d}f\mathrm{d}\xi
\end{aligned} \tag{28}$$

where $H(f)$ is the Fourier Transform of $h(t)$ and $G(f)$ is the Fourier Transform of $g(t)$.

Given that (28) holds for any M large enough to span the support of the receive filter, the limit of (28) may be evaluated as M approaches infinity. This is done using the following identity [31]:

$$\lim_{M\to\infty}\frac{\sin\left[\pi(f-\xi)(2M+1)T_r\right]}{\pi f} \equiv \delta(f-\xi)\ . \tag{29}$$

This is substituted into (28) as follows:

$$\begin{aligned}
E\left[|y|^2\right] &= \lim_{M\to\infty} E\left[|y|^2\right] \\
&= \frac{P_r}{T_s T_r}\int_{-\infty}^{\infty}\int_{-\infty}^{\infty} H^*(f)H(\xi)G(f)G^*(\xi) \\
&\quad \times \sum_{k=0}^{N-1} E\left[|\alpha_k|^2\right] e^{-j2\pi(f-\xi)\tau_k}\delta(f-\xi)\mathrm{d}f\mathrm{d}\xi \\
&= \frac{P_r}{T_s T_r}\int_{-\infty}^{\infty} |H(f)|^2\ |G(f)|^2\mathrm{d}f \\
&= \int_{-\infty}^{\infty}\frac{|H(f)|^2}{T_s}\ R(f)\mathrm{d}f
\end{aligned} \tag{30}$$

where $R(f) \equiv \frac{P_r|G(f)|^2}{T_r}$ is interfering signal PSD [27]. If a matched filter is employed, (30) further reduces to

$$E\left[|y|^2\right] = \frac{1}{P_h}\int_{-\infty}^{\infty} S(f)R(f)\mathrm{d}f \tag{31}$$

where P_h is the power of the desired signal, and $S(f) \equiv \frac{P_h|H(f)|^2}{T_s}$ is the PSD of the desired signal.

ACKNOWLEDGMENT

Research sponsored by the Laboratory for Telecommunications Sciences, US Department of Defense.

"The views expressed in this paper are those of the authors and do not reflect the official policy or position of the United States Air Force, Department of Defense, or the U.S. Government."

REFERENCES

[1] P. Mannion, "Sharing spectrum the smarter way," *EE Times*, April 2004.

[2] I. Akyildiz, W. Lee, M. Vuren, and S. Mohanty, "Next generation / dynamic spectrum access / cognitive radio wireless networks: A survey," *Elsevier Computer Networks*, vol. 50, May 2006.

[3] N. Devroye and P. Mitran, "Achievable rates in cognitive radio channels," *IEEE Transactions on Information Theory*, vol. 52, no. 5, May 2006.

[4] S. Haykin, "Cognitive radio: Brain-empowered wireless communications," *IEEE Journal on Selected Areas in Communciations*, vol. 23, no. 2, pp. 201–220, February 2005.

[5] R. V. Prasad, P. Pawelczak, J. A. Hoffmeyer, and H. S. Berger, "Cognitive functionality in next generation wireless networks: standardization efforts," *IEEE Communications Magazine*, vol. 46, no. 4, June 2008.

[6] A. R. S. Bahai and B. R. Saltzberg, *Multi-Carrier Digital Communications: Theory and Applications of OFDM*. Norwell, MA: Kluwer, 1999.

[7] V. D. Chakravarthy, A. K. Shaw, M. A. Temple, and J. P. Stephens, "Cognitive radio - an adaptive waveform with spectral sharing capability," in *IEEE Wireless Communications and Networking Conference*, 2005.

[8] R. Kannan, Z. Wu, S. Wei, V. Chakravarthy, and M. Rangaswamy, "Soft-decision cognitive radio power control based on intelligent spectrum sensing," in *IEEE Waveform Diversity and Design Conference*, 2007.

[9] Z. Wu and B. Natarajan, "Interference tolerant agile cognitive radio: Maximize channel capacity of cognitive radio," in *4th IEEE Consumer Communications and Networking Conference*, 2007.

[10] M. L. Roberts, M. A. Temple, M. E. Oxley, R. F. Mills, and R. A. Raines, "A general analytic framework for spectrally modulated, spectrally encoded signals," in *IEEE International Conference on Waveform Diversity and Design*, January 2006.

[11] M. L. Roberts, M. A. Temple, R. F. Mills, and R. A. Raines, "Communication waveform design using an adaptive smse framework," *IEEE Journal on Selected Topics in Signal Processing*, vol. 1, no. 1, June 2007.

[12] E. C. Like, M. A. Temple, and S. C. Gustafson, "Adaptive Intra-Symbol SMSE Waveform Design Amidst Coexistent Primary Users," in *IEEE Int'l Conf on Communications (ICC 2009)*, June 2009.

[13] ——, "Intra-Symbol SMSE Waveform Design Amidst Coexistent 802.11 OFDM Signals," in *IEEE Int'l Waveform Diversity & Design Conf (WDD 2009)*, February 2009.

[14] R. G. Gallager, *Information Theory and Realiable Communication*. New York: Wiley, 1999.

[15] A. Batra, S. Lingam, and J. Balakrishnan, "Multi-band ofdm: A cognitive radio for uwb," in *IEEE International Symposium on Circuits and Systems*.

[16] *IEEE Standard for Information technology Telecommunications and information exchange between systems Local and metropolitan area networks Specific requirements Part 11: Wireless LAN Medium Access Control (MAC) and Physical Layer (PHY) Specifications*, IEEE Computer Society, 2007.

[17] S. Honda, D. Umehara, T. Hayasaki, S. Denno, and M. Morikura, "A fast bit loading algorithm synchronized with commercial power supply for in-home plc systems," in *IEEE International Symposium on Power Line Communications and Its Applications*, April 2008.

[18] D. Hughes-Hartogs, "Ensemble modem structure for imperfect transmission media," U.S. Patent Numbers. 4,731,816, March 1988.

[19] B. S. Krongold, K. Ramchandran, and D. L. Jones, "Computationally efficient optimal power allocation algorithms for multicarrier communication systems," *IEEE Transactions on Communications*, vol. 48, no. 1, 2000.

[20] Z. Hu, G. Zhu, Y. Xia, and G. Liu, "Multiuser subcarrier and bit allocation for mimo-ofdm systems with perfect and partial channel information," in *IEEE Wireless Communications and Networking Conference*, vol. 2, March 2004.

[21] J. Jang, K. B. Lee, , and Y.-H. Lee, "Transmit power and bit allocations for ofdm systems in a fading channel," in *IEEE Global Telecommunications Conference*, 2003.

[22] S. Ye, R. Blum, and J. Cimini, L.J., "Adaptive modulation for variable-rate ofdm systems with imperfect channel information," in *IEEE Vehicular Technology Conference*, 2002.

[23] C. Y. Wong, R. S. Cheng, K. B. Letaief, and R. D. Murch, "Multiuser ofdm with adaptive subcarrier, bit and power allocation," *IEEE Journal on Selected Areas of Communications*, vol. 17, October 1999.

[24] V. Chakravarthy, Z. Wu, A. Shaw, M. Temple, R. Kannan, and F. Garber, "A General Overlay/Underlay Analytic Expression for Cognitive Radio Waveforms," in *International Waveform Diversity and Design Conference*, 2007.

[25] V. Chakravarthy, Z. Wu, M. Temple, F. Garber, and X. Li, "Cognitive radio centric overlay-underlay waveform," in *3rd IEEE Symposium on New Frontiers in Dynamic Spectrum Access Networks*, 2008.

[26] V. Chakravarthy, Z. Wu, M. Temple, and F. Garber, "Novel Overlay/Underlay Cognitive Radio Waveforms Using SD-SMSE Framework to Enhance Spectrum Efficiency - Part I," *IEEE Trans on Communciations*, To Appear, Jun 2009.

[27] B. Sklar, *Digital Communications: Fundamentals and Applications*, 2nd ed. New Jersey: Prentice Hall, 2000.

[28] T. W. Beard, M. A. Temple, and M. L. Roberts, "An Experimental Design Approach for Optimizing SMSE Waveforms to Minimize Coexistent Interference," in *IEEE International Conference on Communications*, June 2007, pp. 5581–5585.

[29] T. W. Beard, M. A. Temple, J. O. Miller, R. F. Mills, and J. F. Raquet, "Using Genetic Algorithms for Spectrally Modulated Spectrally Encoded Waveform Design," in *IEEE International Conference on Waveform Diversity and Design*, June 2007, pp. 265–269.

[30] T. W. Beard and M. A. Temple, *C-V-8: Coexistent SMSE Waveform Design Using Optimization*. SciTech Publishing, 2008.

[31] H. J. Weaver, *Theory of Discrete and Continuous Fourier Analysis*. New York: Wiley, 1989.